Journal of Organometallic Chemistry, 302 (1986) 127–146
Elsevier Sequoia S.A., Lausanne – Printed in The Netherlands

MOLECULAR ORBITAL CALCULATIONS ON PLATINUM–GOLD HETEROMETALLIC CLUSTERS

DAVID I. GILMOUR and D. MICHAEL P. MINGOS*
Inorganic Chemistry Laboratory, University of Oxford, South Parks Road, Oxford OX1 3QR (Great Britain)

(Received August 27th, 1985)

Summary

The bonding in some platinum–gold cluster compounds has been analysed using semi-empirical molecular orbital calculations. In $[PtAu_2(PR_3)_4Cl]^+$ (I) and $[Pt_2Au_2(PR_3)_4(CNR')_4]^{2+}$ (II) the platinum–gold bonding involves three-centre two-electron bonds between the bonding orbital of the $Au_2(PR_3)_2$ dimer and the frontier orbitals of the T-shaped platinum fragments. The observed distortions in II have been satisfactorily rationalised. In $[Pt_3Au(\mu\text{-}CO)_3(PR_3)_4]^+$ (III) and $[Pt_3Au(\mu\text{-}SO_2)_2Cl(PR_3)_4]$ (IV) the $AuPR_3^+$ fragments cap the Pt_3 triangles by utilising the acceptor orbital of a_1 symmetry localised on gold. The observed differences in bond lengths for these 54 and 56 electron clusters have been accounted for on the basis of the reduced overlap populations.

Introduction

The bonding in gold and platinum clusters has been analysed using molecular orbital calculations and formed the basis of several interesting stereochemical predictions [1,2]. Recently, several novel heterometallic clusters of these metals have been structurally characterised [3] and representative examples of such compounds are illustrated in I to V.

In I and II the clusters are based on T-shaped PtL_3 fragments and in II, there is no direct metal–metal bonding between the platinum atoms. In III–V, $AuPR_3^+$ fragments cap either 42 or 44 electron Pt_3 triangular clusters based on $[Pt_3(CO)_3(PCy_3)_3]$ or $[Pt_3(SO_2)_2Cl(PCy_3)_3]^-$. These triangular clusters can be viewed in terms of three T-shaped PtL_3 fragments sharing common bridging ligands. The

0022-328X/86/$03.50

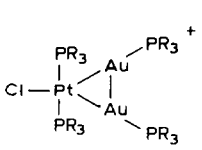

(I)

40 valence electrons

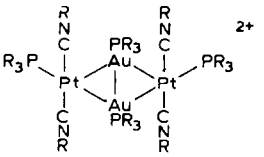

(II)

56 valence electrons

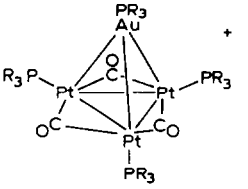

(III)

54 valence electrons

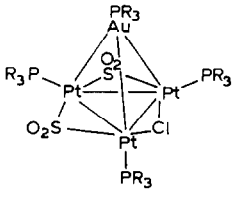

(IV)

56 valence electrons

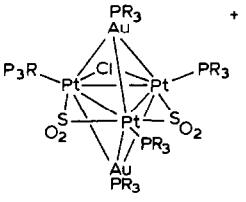

(V)

68 valence electrons

bonding in such triangular clusters has been discussed previously by several groups [4–6]. This paper describes the bonding in the clusters of types I–V.

Bonding in clusters I and II

The T-shaped PtL_3^+ (L is a 2e donor) fragment is *isolobal* with $AuPR_3$, H, CH_3 and metal carbonyl fragments which possess only a single frontier orbital of a_1 symmetry, e.g. $Mn(CO)_5$ [2]. Figure 1 shows the orbitals of a T-shaped PtL_3 fragment. (The ligand L has been modelled by a pseudo-hydrogen H^- for computational reasons). The a_1 orbital is mainly a *dp* hybrid pointing towards the missing vertex of the platinum square-planar coordination polygon. The capability of the PtL_3^+ fragment for forming either localised or multicentred bonding is illustrated in

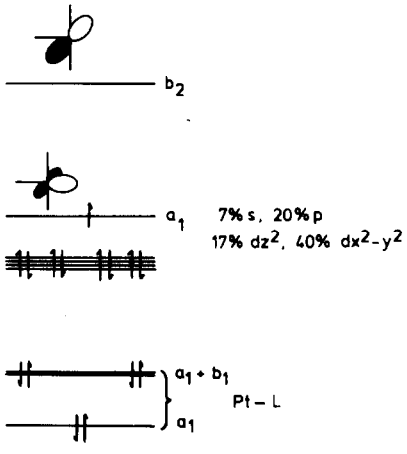

Fig. 1. Frontier molecular orbitals for a T-shaped PtL_3^+ fragment.

VI and VII. The bonding properties of the $AuPR_3$ fragment is similarly determined by an outpointing a_1 hybrid orbital [22].

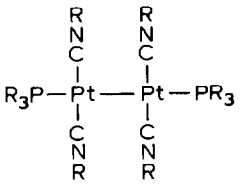

(VI)

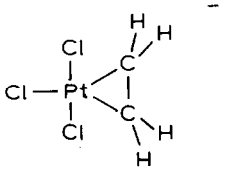

(VII)

In I, the PtL_3 unit symmetrically bridges the $Au_2(PPh_3)_2$ moiety giving a trigonal bipyramidal geometry about platinum and therefore is structurally analogous to the olefin complex VII. Figure 2 illustrates the frontier orbitals of an Au_2L_2 fragment

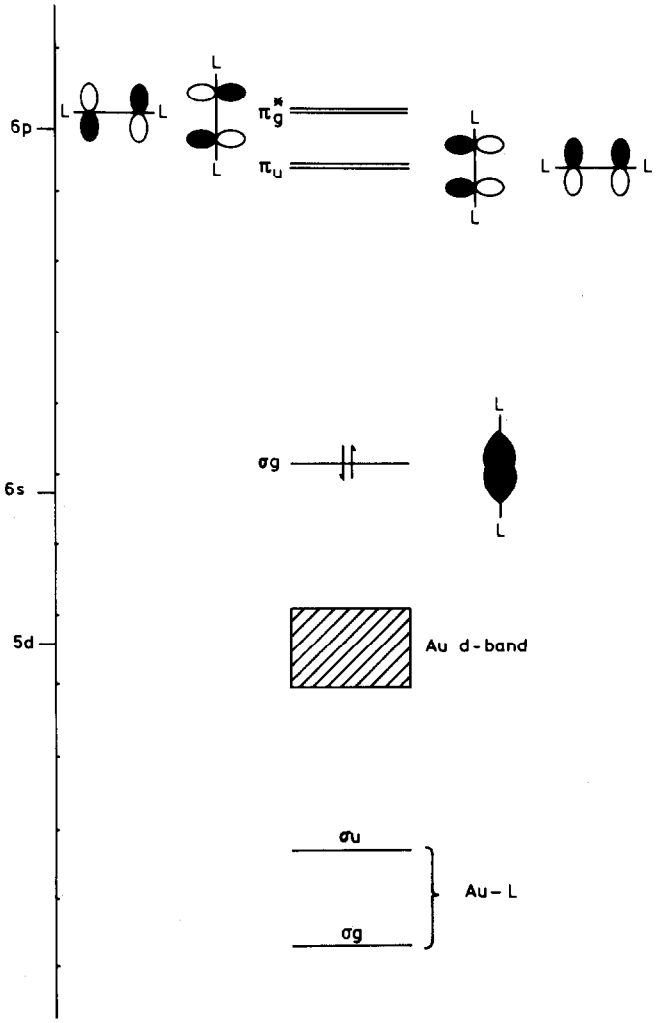

Fig. 2. Frontier orbitals of an Au_2L_2 fragment.

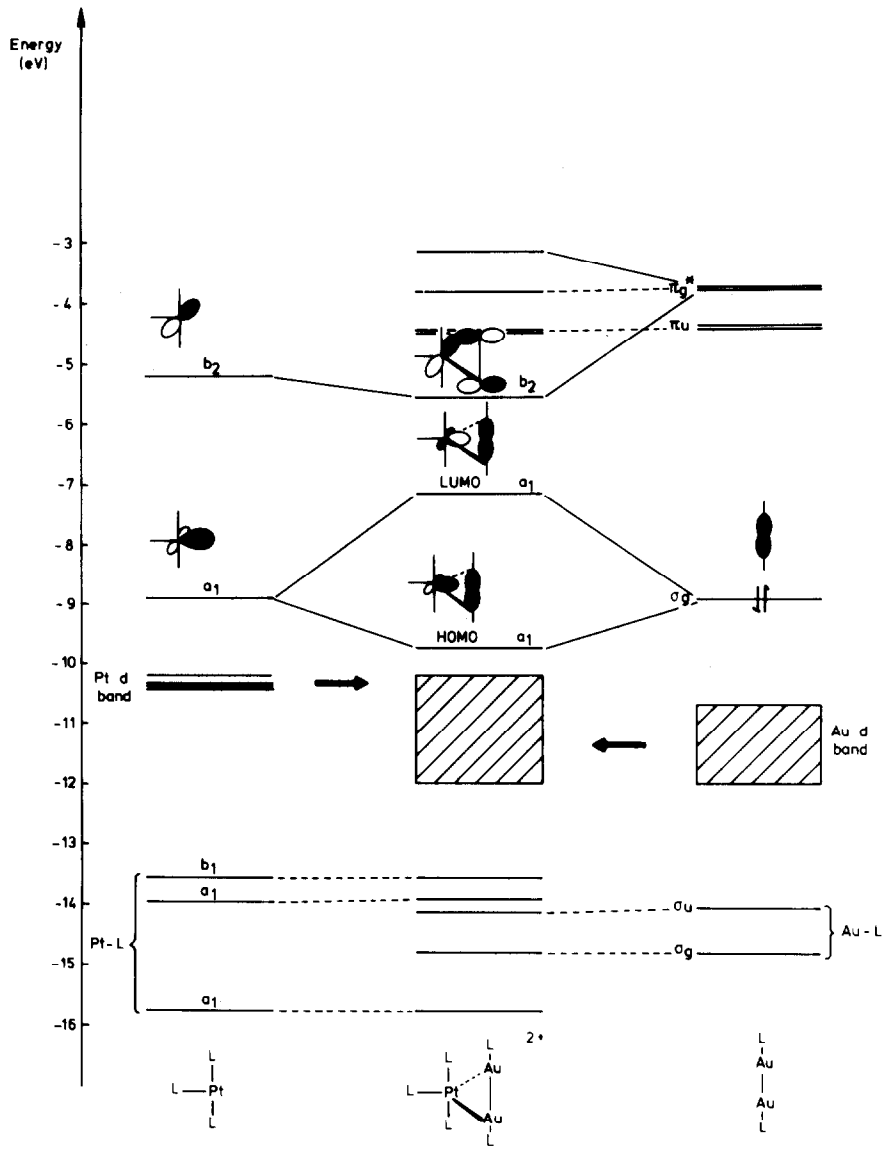

Fig. 3. Interaction diagram for the PtL_3 fragment with the Au_2L_2 fragment.

which serves as a model for $Au_2(PPh_3)_2$. The σ_g Au–Au bonding orbital is the in-phase combination of sp_z orbitals on each gold leading to strong σ-bonding between the gold atoms. At higher energy the π-set form the in-phase (π_u) and the out of phase (π_g^*) combinations of the tangential gold $6p$ orbitals (p_x, p_y). In Au_2L_2, the highest occupied orbital is σ_g.

Figure 3 shows an interaction diagram for the PtL_3 moiety with the Au_2L_2 molecule. The main bonding interaction arises from the formation of a 3-centre 2-electron bond derived from the overlap of the a_1 dp hybrid on PtL_3 with the σ_g orbital of the Au_2L_2 dimer. Bending the Au_2L_2 fragment such that the Au–L

vectors point towards the centroid of the $PtAu_2$ triangle stabilises the 3-centre-2-electron bond by 0.05 eV. This results from an increase in the overlap of the a_1 orbital on PtL_3 with the σ_g orbital on Au_2L_2 and is reflected in the computed reduced overlap populations shown below:

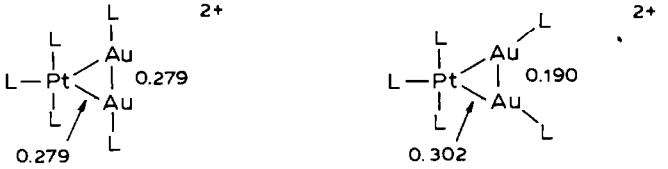

The computed overlap populations show the increase in Pt–Au bonding and decrease in Au–Au bonding as the Au_2L_2 fragment is bent from linearity. The following bond lengths found for $[PtAu_2(PEt_3)_2(PPh_3)_2Cl]^+$ Pt–Au 2.601(4) av. and Au–Au 2.737(3) Å are consistent with this analysis [3b]. The computed reduced overlap population for Au_2L_2 is 0.615 and on coordination to PtL_3 the reduced overlap population falls to 0.190. The main source of gold–gold bonding in I results from $6s$–$6s$ overlap in the HOMO which has 20% Au $6s$ character. The bond lengthening is analogous to that found for the coordination of ethylene to $[PtCl_3]^-$ although there are differences in detail, the C–C bond lengthening is due to a combination of forward and back donation effects, whereas for the Au_2L_2 fragment lengthening occurs from donation from the filled Au–Au σ_g orbital.

In II two PtL_3 fragments are coordinated to a linear Au_2L_2 fragment. The symmetrical disposition of these fragments would lead to a D_{2h} skeletal geometry but an X-ray crystallographic analysis of $[Pt_2Au_2(PPh_3)_4(CN\text{-xylyl})_4]^{2+}$ has revealed a significant distortion which involves a displacement of the platinum atoms towards one of the gold atoms [7] (see VIIIb).

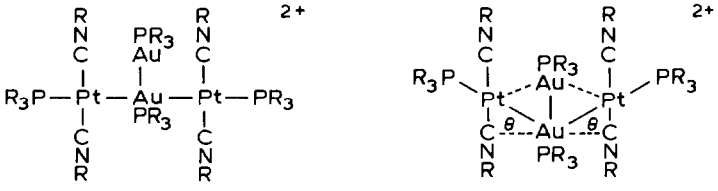

(VIIIa) (VIIIb)

An extension of this distortion would in the limit result in the Au^I/Au^{III} mixed valence compound illustrated in VIIIa.

Figure 4 shows a plot of total energy vs. the distortion coordinate defined by θ in VIIIb. Even though the ligands have been modelled in a simple fashion, the calculation shows a broad minimum for $\theta = 20$–$25°$. The observed value of θ determined from the crystal structure analysis is 22.51(6)°. The plot also emphasises that II and VIIIb are connected by a soft potential energy surface, which is consistent with the NMR data for this compound in solution [7]. Figure 5 shows an interaction diagram for II derived by symmetrically bridging the Au_2L_2 dimer with two PtL_3 fragments. The primary bonding interactions arise through the a_g orbital, a 4-centre 2-electron bond which has 31% Pt and 46% Au character. The gold is sp hybridised (24%s, 14%p) and overlap of the two Au sp hybrids leads to strong Au–Au bonding. Occupation of the a_g orbital leads to an Au–Au reduced overlap population of 0.23 compared with 0.19 for $[PtAu_2L_5]^+$. This difference in reduced

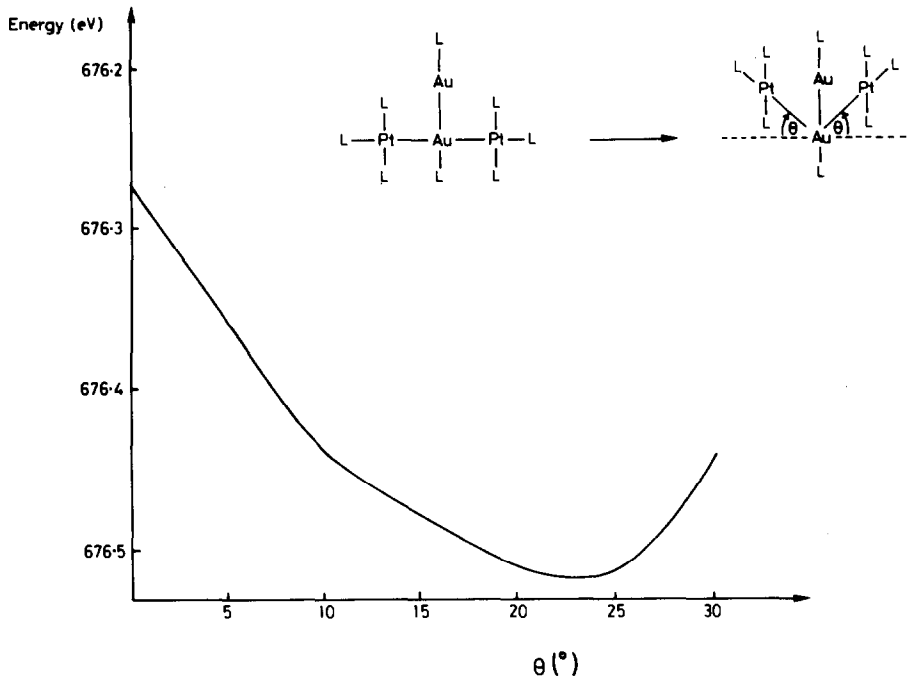

Fig. 4. Plot of total energy vs. the distortion coordinate.

overlap populations is reflected in the shorter Au–Au bond length for $[Pt_2Au_2(PPh_3)_4(CN\text{-xylyl})_4]^{2+}$ of 2.593(2) Å compared with 2.737(3) Å in $[PtAu_2(PPh_3)_2(PEt_3)_2Cl]^+$. A small stabilisation of the Au $5d$ band is also observed. This can be attributed primarily to a stabilisation of the b_{3u} orbital which has mainly Au $5d_{xz}$ character (Au 90% and 3% Pt), this orbital stabilised by approximately 0.1 eV by overlap with the out-of-phase combination of PtL_3 moieties.

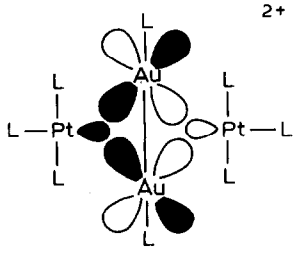

The HOMO in II is of b_{3u} symmetry and is almost non-bonding with respect to the Au_2L_2 unit. This orbital has 60% Pt and only 8% Au character and can be described as an out-of-phase combination of platinum dp hybrids. The gold $6p$ contribution to this molecular orbital is not large because the energy match between the platinum dp hybrids and the gold $6p$ orbitals is not a good one. The LUMO is of a_g symmetry and arises from an in-phase combination of PtL_3 units overlapping out-of-phase with a_g orbital of the Au_2L_2 dimer.

In valence bond terms the bonding in $[Pt_2Au_2L_8]^{2+}$ can be described in terms of a pair of 3-centre 2-electron bonds associated with each of the Au_2Pt triangles. The

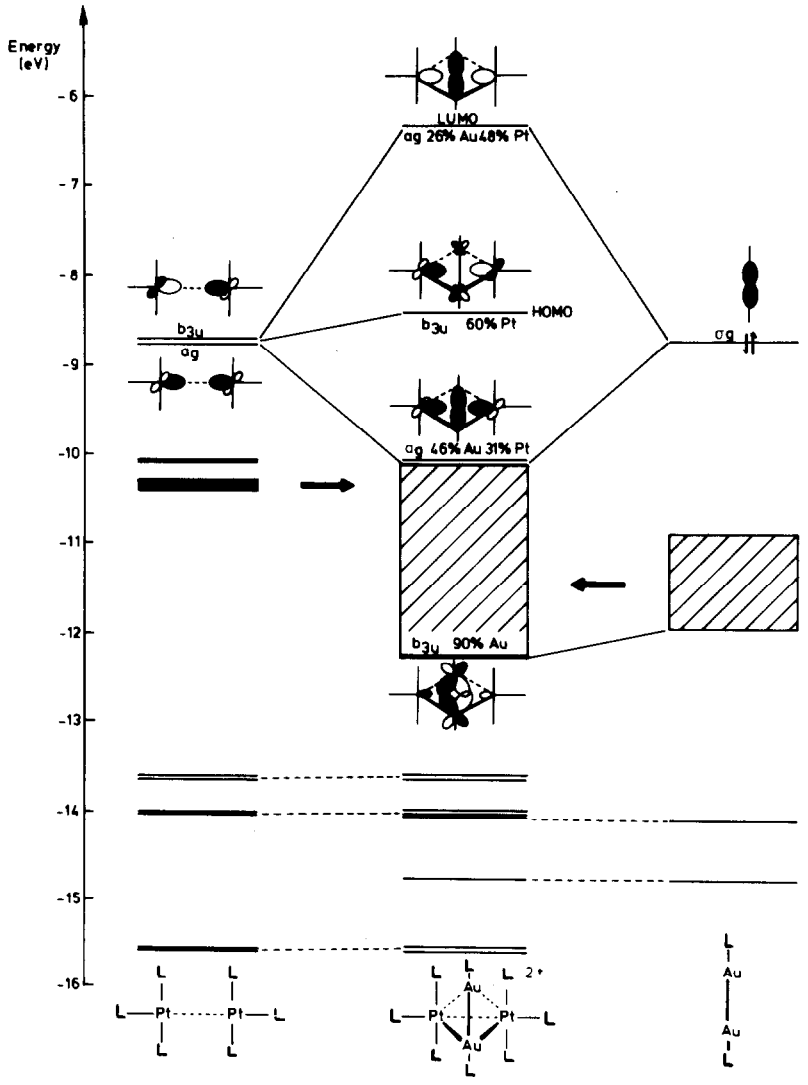

Fig. 5. Interaction diagram for two PtL_3 fragments with the Au_2L_2 fragment. The calculation is based on a symmetrical D_{2h} geometry.

symmetrised molecular orbital equivalents of these localised orbitals shown in IXa and IXb resemble the a_g and b_{3u} molecular orbitals shown in Fig. 5, but such a localised view of the bonding over-emphasises the contribution of IXb.

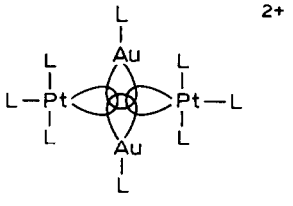

(IXa)

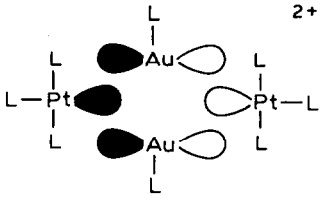

(IXb)

The small contribution of the gold $6p$ orbitals to b_{3u} in Fig. 5 influences the soft nature of the potential energy surface connecting VIIIa and the symmetrical D_{2h} structure.

Figure 6 shows a Walsh diagram for this distortion mode. The a_g bonding orbital is destabilised due to loss of overlap of the platinum dp hybrids with the Au–Au σ_g

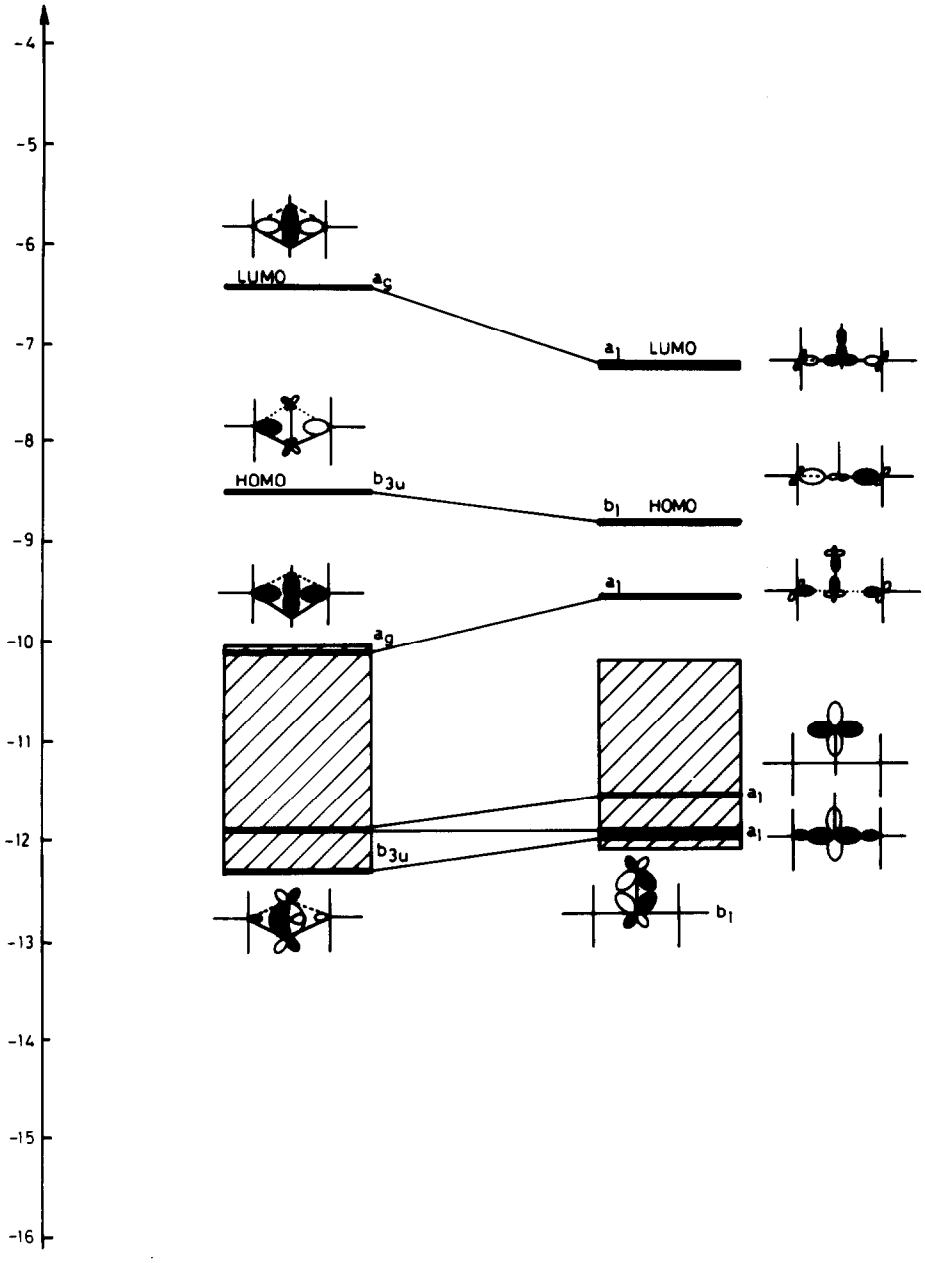

Fig. 6. Walsh diagram for distortion from D_{2h} to C_{2v} for $[Pt_2Au_2L_8]^{2+}$.

orbital, the *dp* hybrids interacting with a Au–Au $d_{x^2-y^2}$ combination which is Au–Au bonding but Pt–Au anti-bonding. The HOMO of b_{3u} symmetry is slightly stabilised due to improved overlap of the *dp* hybrids with the gold 6*p* orbital. This orbital has 76% Pt and 9% Au character. The LUMO of a_g symmetry is stabilised because of loss of overlap of the Pt *dp* hybrids with the Au–Au σ bond. Small destabilisations of the Au 5*d* band also occur – the Au–Au bonding d_{xy} combination is destabilised due to loss of overlap of the Pt *dp* hybrids and also the Au–Au $d_{x^2-y^2}$ combinations change in energy on distortion (see Fig. 6). From the relative

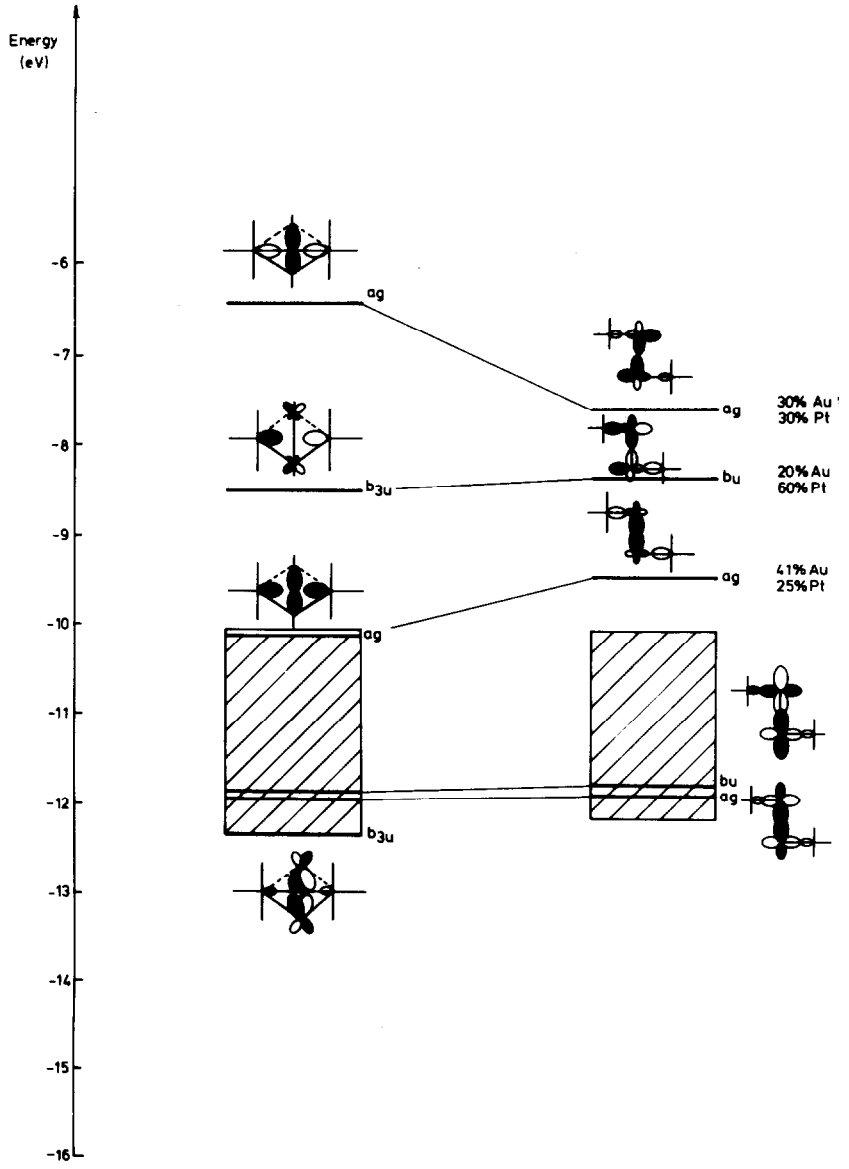

Fig. 7. Walsh diagram for distortion from D_{2h} to C_{2h} for $[Pt_2Au_2L_8]^{2+}$.

slopes of the levels in Fig. 6 it is apparent that the larger positive slopes of a_g–a_1 leads to a preference for structures with large θ values. However, the potential energy surface is soft near the symmetric structure (θ 30°) because the relative effects of the a_g and b_{3u} stabilisation have a cancelling effect. Indeed up to θ 22.5° the latter effect slightly outweighs the former leading to the observed minimum at θ 22.51(6)°.

An alternative distortion pathway resulting in a C_{2h} skeletal geometry can also be considered:

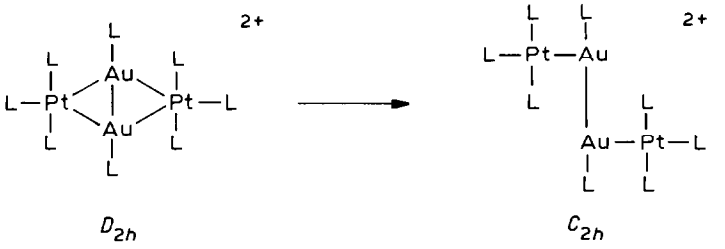

This type of transformation resembles that generally observed for carbonyl complexes, where bridge-terminal exchange has a very low activation energy [8].

Figure 7 shows a Walsh diagram for such a distortion mode. The energies of the molecular orbitals change dramatically. The LUMO is stabilised and the bonding a_g is destabilised as a result of loss of overlap between the platinum *dp* hybrids and the gold σ_g molecular orbital. In contrast with the situation for the D_{2h}–C_{2v} distortion the HOMO (b_{3u}) is not stabilised.

In valence bond terms the gold atom has been rehybridised to form two T-shaped Au^{II} fragments with the outpointing hybrids pointing to the missing vertex of the square plane about gold. It is therefore a diradical species. The molecular orbital equivalent as represented in Fig. 7 is the pair of molecular orbitals b_{3u} and a_g which are closely spaced in energy.

Bonding in clusters III–V

The platinum–gold clusters III–V are all based on triangular $[Pt_3(\mu\text{-}X)_3(PR_3)_3]$ units which have either been capped by one $AuPR_3^+$ fragment leading either to 54 or 56 valence electron tetrahedral clusters (e.g. III and IV) or alternatively by two $AuPR_3^+$ fragments leading to 68 valence electron trigonal bipyramidal clusters (e.g. V). It is therefore instructive to discuss the bonding in III to V in terms of the frontier orbitals of the parent triangular clusters. An important feature of the parent triangular clusters is their ablility to exhibit electron counts of either 42 or 44 valence electrons. Several research groups have discussed the electronic reasons for these alternative electron counts [4–6] and therefore only a brief account of the bonding in the parent triangular cluster will be given below.

A localised view of the bonding in $[Pt_3(\mu\text{-}X)_3(PR_3)_3]$ leads to a valence electron count of 42 corresponding to the attainment of 16 electron configurations about each of the platinum atoms. The three localised Pt–Pt bonds correspond approximately to the occupation of an e' and a'_1 set of orbitals which can be derived from the frontier orbitals of three PtL_2 fragments arranged in a triangular and planar fashion (see Fig. 8). In addition, these clusters are characterised by a pair of low

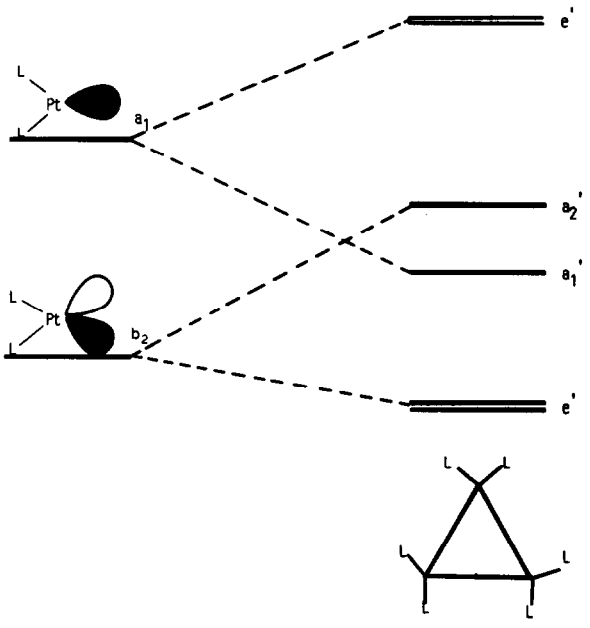

Fig. 8. Skeletal molecular orbitals for Pt_3L_6.

lying orbitals of a_2' (Pt–Pt antibonding) and a_2'' symmetry. The latter molecular orbital has some metal $6p$ character but also has significant contributions from the unoccupied molecular orbitals of the bridging and terminal ligands. The a_2'' and a_2' molecular orbitals are illustrated schematically in Xa and Xb.

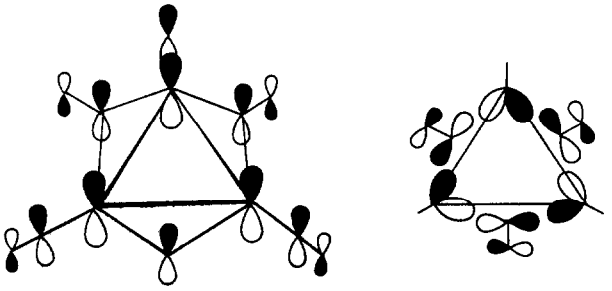

(Xa) (Xb)

These molecular orbitals can accommodate an additional electron pair if they are stabilised in an effective fashion by the bridging ligands. Figure 9 illustrates the orbital energies of $[Pt_3(\mu\text{-}X)_3(PR_3)_3]$ ($X = CO$, SO_2 and PH_2^+) and suggests the energies of the a_2' and a_2'' orbitals are sensitive to the energies and symmetries of the acceptor orbitals of the bridging groups [4]. For the carbonyl ligand, both orbitals are effectively degenerate because CO is a cylindrically symmetric ligand. In contrast SO_2 and PH_2^+ both have only a single acceptor orbital and when the ligands are

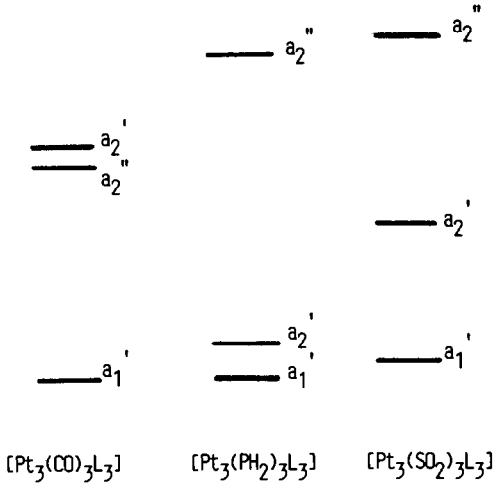

Fig. 9. Orbital energies of $Pt_3(\mu\text{-}X)_3L_3$ (X = CO, SO_2 and PH_2^+).

oriented as shown in XI, the acceptor orbitals lie in the Pt_3 plane and stabilise the a_2' unoccupied orbital.

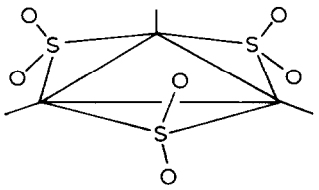

(XI)

The formation of 44 electron clusters based on the occupation of this in-plane orbital is particularly favoured by the introduction of ligands such as PH_2^+ which have a low lying π-acceptor level. Since the a_2' molecular orbital is somewhat antibonding between the metals the computed platinum–platinum overlap populations for the 44 electron clusters are smaller than those for the 42 electron clusters.

Figure 10 illustrates the principal orbital interactions between $[Pt_3(SO_2)_3L_3]$ and a capping AuL^+ fragment. The major bonding interactions arise between the a_1 orbital of the AuL^+ fragment and orbitals with matching symmetry properties on the platinum triangle. The a_1 HOMO of the platinum triangle which has a high percentage of platinum 6*s* character and the lower lying orbital of a_1 symmetry with predominately d_{z^2} character are particularly important in this respect. These orbital interactions are improved if the ligands on the platinum triangle are bent away from the capping gold atom because of the greater overlaps between the apical atom orbitals with the Pt_3 orbitals. Distortions of this type are observed in the solid state for $[Pt_3(\mu\text{-}CO)_3(PPh_3)_3AuPPh_3]^+$ and the related clusters. The interaction of the a_1 orbital of the AuL^+ fragment with the a_2'' molecular orbital of the Pt_3 triangle does not contribute significantly to the skeletal bonding in the cluster as the a_2'' orbital is high lying. The $6p_x$ and $6p_y$ orbitals of the AuL^+ fragment also make very little contribution to the skeletal bonding. Therefore in the Pt_3Au cluster the bonding is best described in terms of an *e* set of orbitals, localised predominantly on the Pt_3

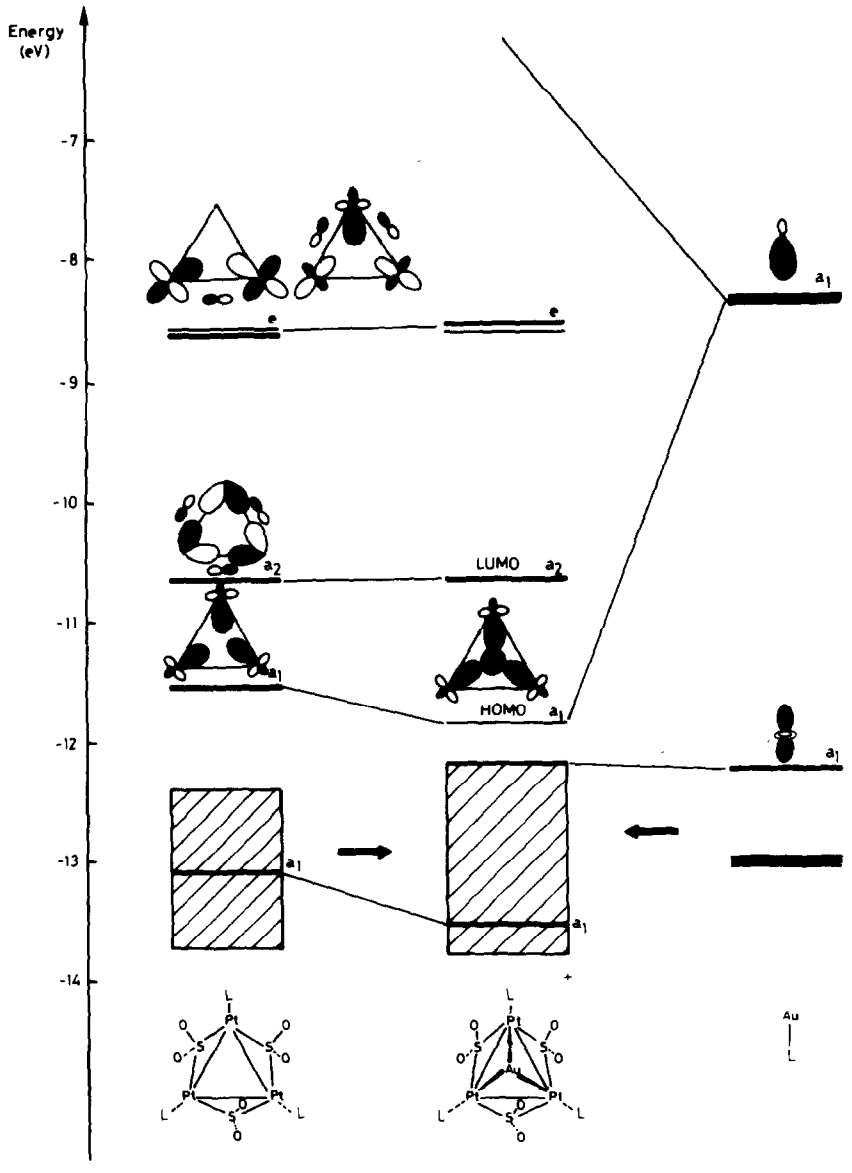

Fig. 10. Interaction diagram for $[Pt_3(SO_2)L_3]$ and capping AuL^+.

triangle and a four-centre two-electron bond involving the a_1 orbitals of both fragments. This situation contrasts with that for the tetrahedral clusters of the earlier platinum metals, e.g. $Ir_4(CO)_{12}$, where six molecular orbitals can be identified with skeletal bonding and the total valence count is 60 rather than 54.

The AuL^+ fragment does not have any frontier orbitals of a_2 symmetry and consequently molecular orbitals of a_2 symmetry of the Pt_3 triangle are unaffected by AuL^+ capping. Therefore the a_2 molecular orbital retains the bonding characteristics noted above for the parent Pt_3 triangular clusters.

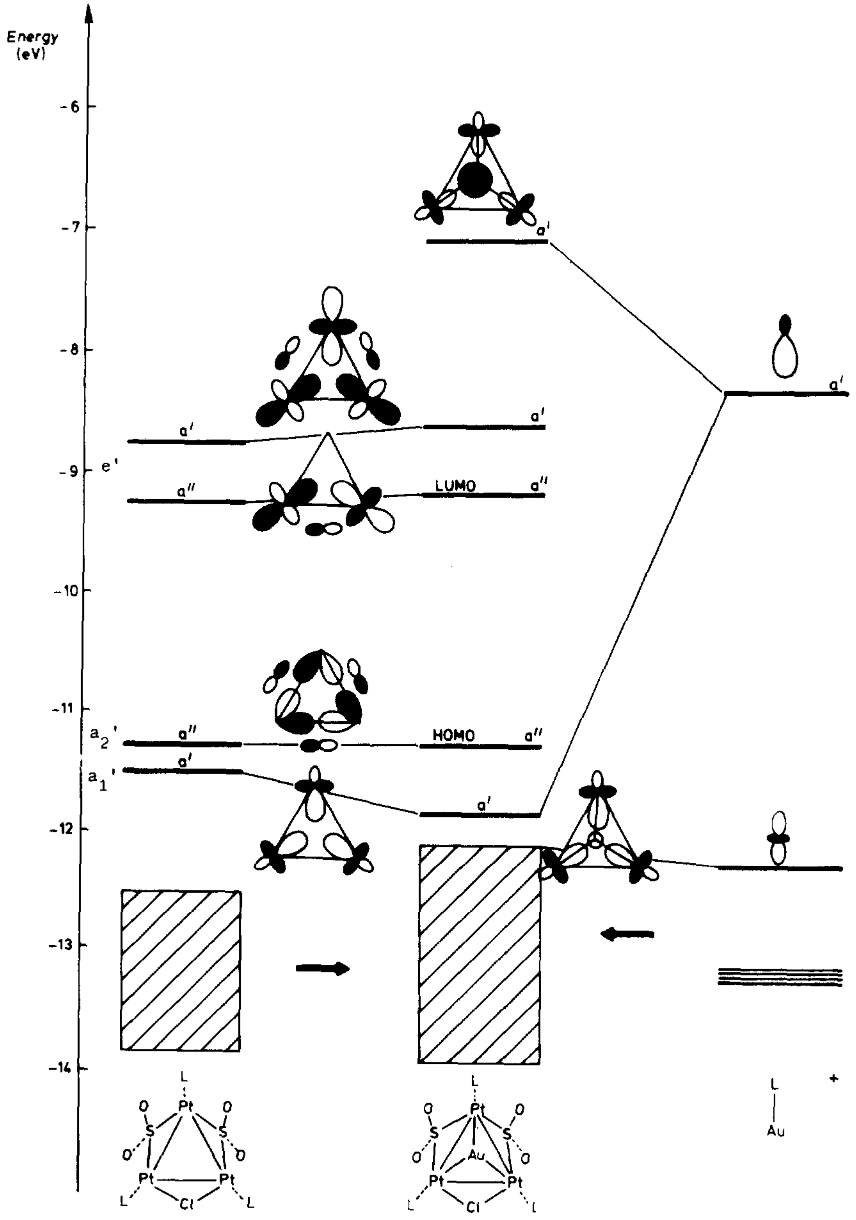

Fig. 11. Interaction diagram for $[Pt_3(SO_2)_2ClL_3]^-$ with AuL^+.

Substitution of one of the bridging SO_2 ligands by either PH_2 or Cl has the effect of stabilising the a_2' orbital in the Pt_3 triangle and also in the capped Pt_3Au cluster. Figure 11 illustrates the interaction diagram for capping the 44 electron triangular cluster $[Pt_3(SO_2)_2ClL_3]^-$ with AuL^+. The stabilisation of the a_2' orbital accounts for the occurrence of the 56 electron cluster. The lower symmetry of this cluster (C_s rather than C_{3v}) results in a removal of degeneracy of the molecular orbitals of e symmetry and a stabilisation of the a'' component.

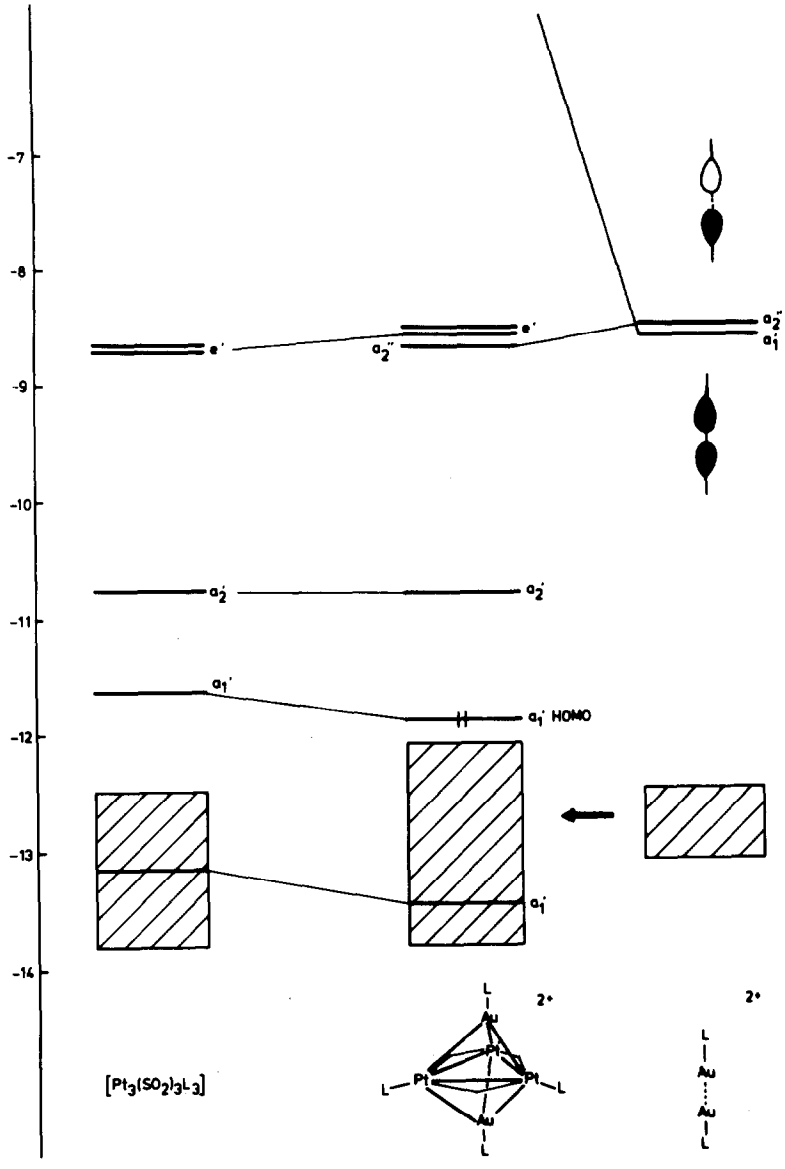

Fig. 12. Orbital interaction diagram for $[Pt_3(SO_2)_3L_3]$ and two capping AuL^+ fragments.

Besides forming 54 and 56 electron Pt_3Au clusters it is possible also to doubly cap the Pt_3 triangle with AuL^+ fragments to generate trigonal bipyramidal Pt_3Au_2 clusters. Figure 12 illustrates the principle orbital interactions between $[Pt_3(SO_2)_3L_3]$ and two capping AuL^+ fragments. The major bonding interactions occur between the a_1' in-phase combination of *sp* hybrids of the AuL^+ fragments and the a_1 same orbitals of the Pt_3 triangle which are utilised in the Pt_3Au tetrahedral clusters. The a_2'' combination of AuL^+ fragments is stabilised by the higher lying a_2'' molecular orbital of the Pt_3 triangle. The interaction between them is not strong because of the

large energy difference between the interacting orbitals. The orbital interaction diagram shown in Fig. 12 retains the three bonding skeletal molecular orbitals of the parent triangular cluster and a low lying orbital of a_2' symmetry. This orbital is stabilised further by the substitution of SO_2 by either PH_2 or Cl ligands. This analysis is consistent with the observation that the only known example of a trigonal bipyramidal Pt_3Au_2 cluster has 4 skeletal electron pairs associated with its 68 valence electrons derived from occupation of the e', a_1' a_2' molecular orbitals, the latter stabilised by a bridging chloride ligand. This contrasts with the situation in trigonal bipyramidal clusters of the earlier platinum metals which posess six skeletal bonding molecular orbitals and a total of 72 valence electrons [6].

The above theoretical analysis has suggested that the capping AuL fragments interact primarily with the Pt_3 triangle through orbitals of a_1 symmetry. In this section the detailed geometric consequences of this model are analysed. The computed reduced overlap populations for $[Pt_3(SO_2)_3(PH_3)_3]$ and $[Pt_3Au(SO_2)_3(PH_3)_4]^+$ are given below:

OVERLAP POPULATIONS

	Pt–Pt	Pt–Au
$[Pt_3(SO_2)_3(PH_3)_3]$	0.186	–
$[Pt_3Au(SO_2)_3(PH_3)_4]^+$	0.161	0.094

They suggest a weakening of the Pt–Pt bonds on capping resulting from the additional delocalisation of the a_1 molecular orbitals onto the gold atom. The small Pt–Au overlap population is consistent with the small contribution made by the gold $6p_x$ and $6p_y$ orbitals to metal–metal bonding.

Table 1 summarises bond length data for the known platinum–gold clusters and related triangulo-Pt_3 clusters.

The data confirms that capping the 42 electron $[Pt_3(\mu\text{-}X)_3L_3]$ cluster by AuL^+ to generate $[Pt_3Au(\mu\text{-}X)_3L_4]^+$ leads to a lengthening of the Pt–Pt bonds. In addition the Pt–Au bonds are longer than the Pt–Pt bonds.

TABLE 1

SUMMARY OF METAL–METAL BOND LENGTHS IN PLATINUM–GOLD CLUSTERS

	Pt–Pt (Å)	Pt–Au (Å)
42 electrons		
$[Pt_3(SO_2)_3(PPh_3)_3]$ [9]	2.695(1)–2.712(1)	–
$[Pt_3(CO)_3(PCy_3)_3]$ [10]	2.653(2)–2.656(2)	–
54 electrons		
$[Pt_3Au(CO)_2(SO_2)(PCy_3)_4]^+$ [3c]	2.667(4)–2.746(1)	2.755(1)–2.759(5)
$[Pt_3Au(CO)_3(PCy_3)_4]^+$ [3a]	2.696(9) av.	2.758(5) av.
56 electrons		
$[Pt_3Au(SO_2)_2Cl(PCy_3)_3\{P(p\text{-}C_6H_4F)_3\}]$	2.851(1)–2.869(1)	2.766(1)–2.771(1)
68 electrons		
$[Pt_3Au_2(SO_2)Cl(PCy_3)_3\{P(p\text{-}C_6H_4F)_3\}_2]^+$	2.884(2)–2.887(2)	2.772(2)–2.803(2)

The computed reduced overlap populations for $[Pt_3(SO_2)_2Cl(PH_3)_3]^-$ and $[Pt_3Au(SO_2)_2Cl(PH_3)_4]$ are summarised below:

OVERLAP POPULATIONS

	Pt–Pt	Pt–Au
$[Pt_3(SO_2)_2Cl(PH_3)_3]^-$	0.142 av.	–
$[Pt_3Au(SO_2)_2Cl(PH_3)_4]$	0.113 av.	0.093 av.

The introduction of the bridging chloride stabilises the a_2' orbital in both the triangular and tetrahedral clusters. This orbital is localised predominantly on the Pt_3 triangle and is metal–metal antibonding. Since the additional electron pair in these clusters resides in this orbital, a weakening of the Pt–Pt bonds results. Its localisation on the Pt_3 triangle results in the Pt–Au overlap population being unaffected by the change in electron count. The bond length data for Table 1 are consistent with these changes in computed reduced overlap populations.

The computed reduced overlap populations for $[Pt_3Au_2(SO_2)_2Cl(PH_3)_5]^+$ are summarised:

OVERLAP POPULATIONS

	Pt–Pt	Pt–Au
$[Pt_3Au_2(SO_2)_2Cl(PH_3)_5]^+$	0.087 av.	0.088 av.

The introduction of an additional capping $Au(PH_3)^+$ fragment to generate the 68 electron cluster causes the diminution of metal–metal bonding resulting from the additional delocalisation of the a_1 orbital over five metal atoms compared with four for the tetrahedral Pt_3Au clusters.

Although the discussion above has focused on trigonal bipyramidal clusters of gold and platinum, the arguments can be extended to the fragments $SnCl_3^+$, $Mo(CO)_5$ and $Ni(CO)_3$ which are *isolobal* [1] with $AuPR_3^+$ and generate structurally similar clusters shown in XII, XIII and XIV.

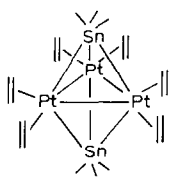

$[Pt_3(COD)_3(SnCl_3)_2]$ [11]
(XII)

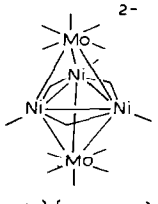

$[\{Ni_3(CO)_6\}\{Mo(CO)_5\}_2]^{2-}$ [12]
(XIII)

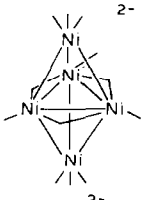

$[Ni_5(CO)_{15}]^{2-}$ [13]
(XIV)

Although the number of skeletal molecular orbitals involved in bonding in XII to XIV is the same as for $[Pt_3Au_2(SO_2)_2Cl(PR_3)_5]^+$, the occupied orbitals do differ in an important and significant fashion. In XII to XIV the ligands attached to the central metal are stronger π-acids and have the correct symmetry to interact with the a_2'' shown in Xa and consequently have the effect of stabilising this molecular orbital. This is shown in Fig. 13 which illustrates the relative energies of the skeletal molecular orbitals for $[M_3L_3(SO_2)_3]$ and $[M_3(CO)_6]^{2-}$. The a_2'' molecular orbital is further stabilised by interaction with the a_2'' combination of the capping fragments (see Fig. 14). The resulting a_2'' orbital which is metal–metal bonding is occupied in the clusters XII to XIV. The bonding in them is best described as a pair of 4-centre

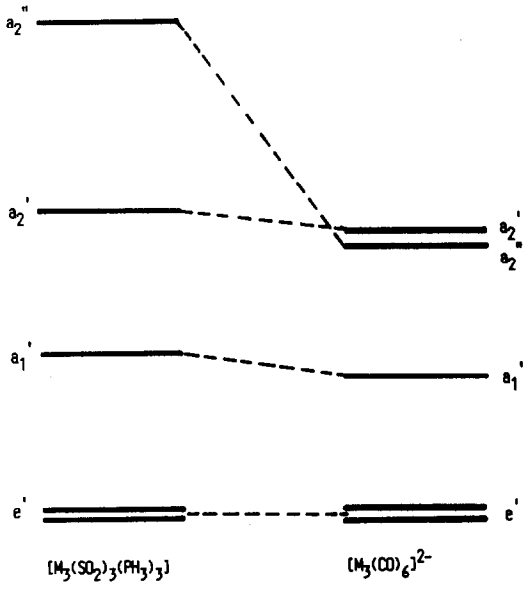

Fig. 13. Relative energies of the skeletal molecular orbitals for $[M_3L_3(SO_2)_3]$ and $[M_3(CO)_6]^{2-}$.

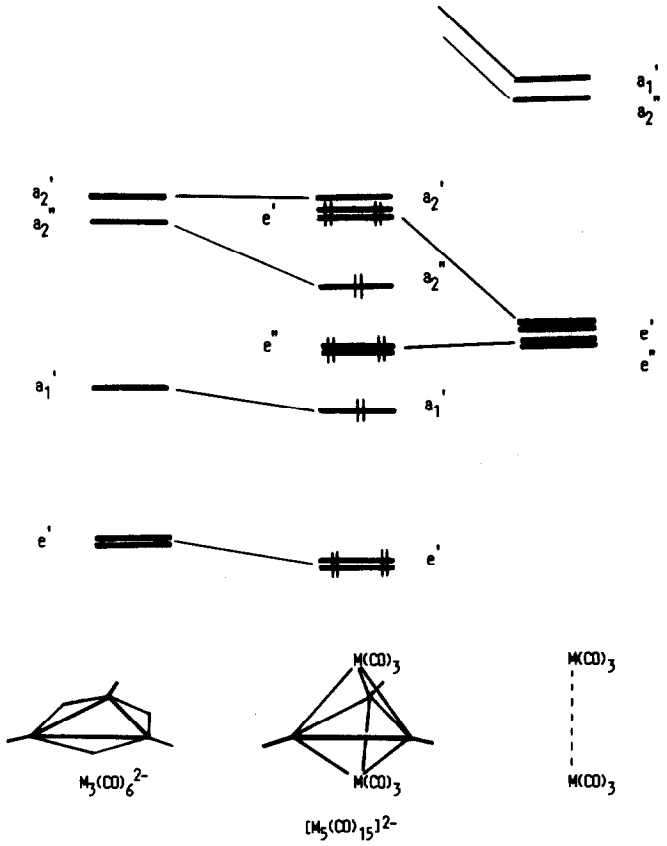

Fig. 14. Interaction diagram for $[M_3(CO)_6]^{2-}$ interacting with two capping $M(CO)_3$ fragments.

2-electron bonds involving the a_1' and a_2'' molecular orbitals of the M_3 triangle. As the metal–metal antibonding a_2' molecular orbital is unoccupied the Pt–Pt bond length of 2.60(1) Å in XII is significantly shorter than the Pt–Pt bond lengths in V.

Figure 14 also shows the e' combination of dp hybrids of the $M(CO)_3$ fragments with e' molecular orbitals of the triangle. The out-of-phase e' molecular orbital is localised mainly on the capping $M(CO)_3$ fragments is antibonding between capping atoms and triangle. In XIII and XIV which have 76 valence electrons this pair of orbitals is occupied. Increasing the axial bond lengths results in the stabilisation of the e' molecular orbital due to loss of overlap of the dp hybrids for the triangular based e' molecular orbitals. This distortion is thus favourable for the $[M_5(CO)_{15}]^{2-}$ clusters and accounts for the asymmetry in the equatorial and axial bond lengths. The bonding in these clusters has also been discussed by several other groups [13–15].

Appendix

All the calculations were performed using the extended Hückel method [16] following the procedures detailed in previous papers [1,7]. The electronic parameters which were used for input into the ICON 8 program are given in Table A1 and A2 below. The geometries of the Pt_2Au and Pt_2Au_2 clusters were modelled with

TABLE A1

PARAMETERS FOR NON-METAL ATOMS

Atom	Orbital	Slater exponent	H_{ii} (eV)
H and L	1*s*	1.30	−13.60
P	3*s*	1.60	−18.60
	3*p*	1.60	−14.00
Cl	3*s*	2.033	−30.00
	3*p*	2.033	−15.00
S	3*s*	1.817	−20.00
	3*p*	1.817	−13.30
O	2*s*	2.275	−32.30
	2*p*	2.275	−14.80

TABLE A2

PARAMETERS FOR METAL ATOMS

Atom	Orbital	H_{ii} (eV)	ζ_1	c_1	ζ_2	c_2
Au	6*s*	− 9.22	2.602			
	6*p*	− 4.27	2.584			
	5*d*	−12.16	6.163	0.648	2.734	0.559
Pt	6*s*	−10.75	2.602			
	6*p*	− 5.27	2.550			
	5*d*	−13.16	6.010	0.6332	2.696	0.551

metal–metal 2.7 and M–L 1.66 Å. For the triangular clusters the calculations were performed with M–M 2.67, M–L 1.7, S–O 1.45, M–S 2.27, M–Cl 2.27 Å. For the PH_3 ligand the P–H bond lengths of 1.45 Å and M–P–H bond angle of 105° were used.

Acknowledgements

The S.E.R.C. is thanked for its financial support. Mrs. C. Palmer is thanked for assistance in producing the diagrams and Figures, and Mr. R.L. Johnston is thanked for helpful discussions.

References

1 D.M.P. Mingos, J. Chem. Soc., Dalton Trans., (1976) 1163.
2 D.G. Evans and D.M.P. Mingos, J. Organomet. Chem., 232 (1982) 171.
3 (a) C.E. Briant, R.W.M. Wardle and D.M.P. Mingos, J. Organomet. Chem., 267 (1984) C49; (b) P. Braunstein, H. Lenner, D. Matt, A. Tiripicchio and M. Tiripicchio-Camellini, Angew. Chem. Int. Ed. Engl., 96 (1984) 307; (c) R.W.M. Wardle and D.M.P. Mingos, J. Chem. Soc., Dalton Trans., (1985) in press; (d) D.M.P. Mingos, D. J. Sherman and P.I. Oster, unpublished results; (e) C.E. Briant, D.I. Gilmour and D.M.P. Mingos, J. Organomet. Chem., 267 (1984) C52.
4 D.J. Underwood, R. Hoffmann, K. Tatsumi, A. Nakamura and Y. Yamamoto, J. Amer. Chem. Soc., (1985) in press.
5 C. Mealli, J. Amer. Chem. Soc., 107 (1985) 2245.
6 N. McEvoy and D.M.P. Mingos, Part II Thesis 1980.
7 C.E. Briant, D.I. Gilmour and D.M.P. Mingos, J. Chem. Soc., Dalton Trans., submitted.
8 F.A. Cotton and G. Wilkinson, Advanced Inorganic Chemistry, 4th Edition J. Wiley and Sons, New York, 1980, p. 1058.
9 D.C. Moody and R.R. Ryan, Inorg. Chem., 16 (1977) 1052.
10 A. Albinati, Inorg. Chim. Acta, 22 (1977) L31.
11 L.J. Guggenberger, J. Chem. Soc., Chem. Commun., (1968) 512.
12 J.K. Ruff, R.P. White and L.F. Dahl, J. Amer. Chem. Soc., 93 (1971) 2159.
13 G. Longoni, P. Chini, L.D. Lower and L.F. Dahl, J. Amer. Chem. Soc., 97 (1975) 5034.
14 J.W. Lauher, J. Amer. Chem. Soc., 100 (1978) 5305.
15 P. Fantucci, G. Pacchioni and V. Valenti, Inorg. Chem., 23 (1984) 247.
16 R. Hoffmann and W. Lipscomb, J. Chem. Phys., 36 (1982) 2179.